Volume 54
Number 20
28 May 2025
Pages 7957-8360

Dalton Transactions

An international journal of inorganic chemistry

rsc.li/dalton

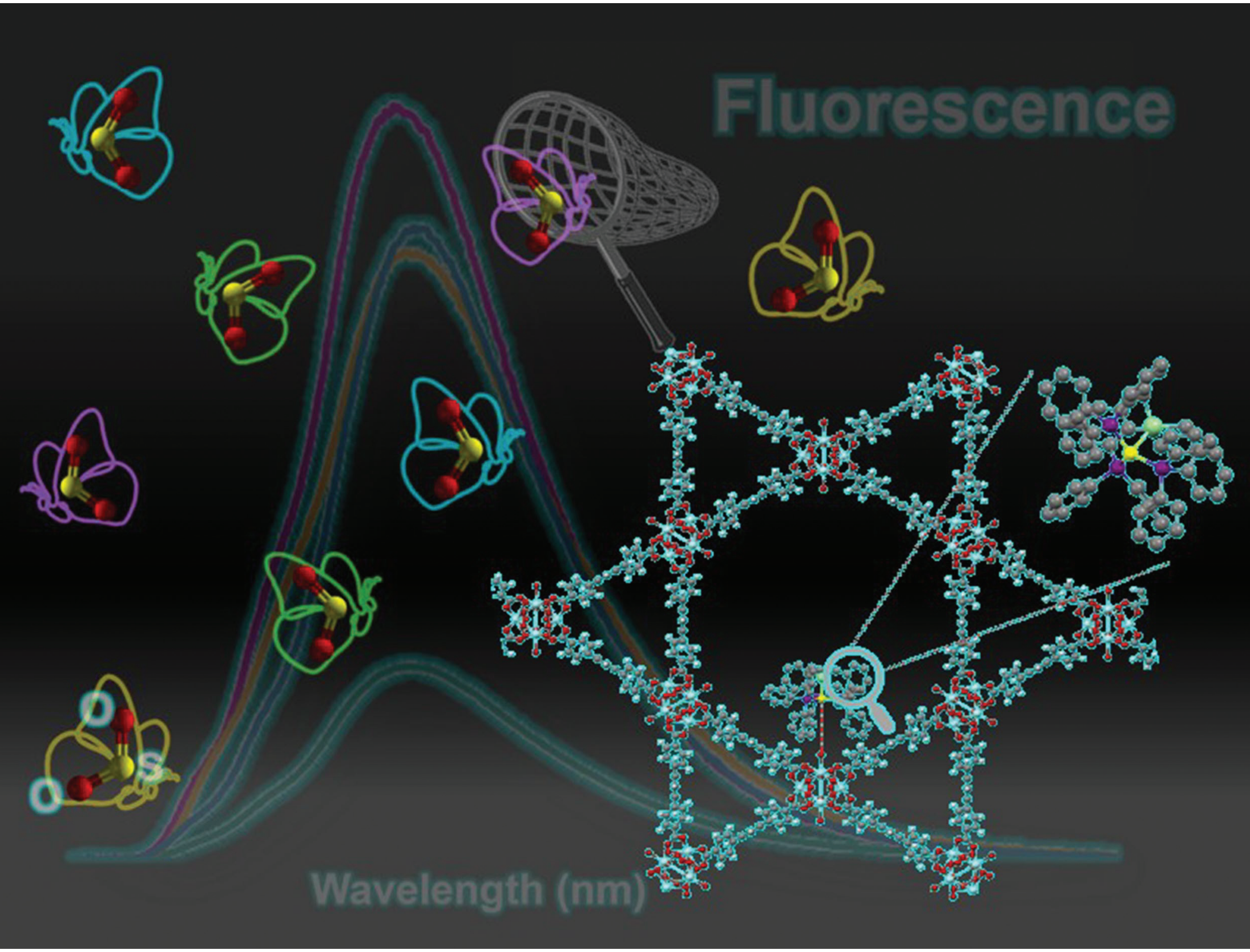

ISSN 1477-9226

ROYAL SOCIETY OF **CHEMISTRY**

COMMUNICATION

Elí Sánchez-González, Ilich A. Ibarra,
Virginia Montiel-Palma *et al.*

Selective detection of SO_2 in NU-1000 *via* organometallic nickel silylphosphine post-synthetic complex incorporation

Dalton Transactions

COMMUNICATION

Cite this: *Dalton Trans.*, 2025, **54**, 8029

Received 11th September 2024,
Accepted 22nd April 2025

DOI: 10.1039/d3dt03985d

rsc.li/dalton

Selective detection of SO_2 in NU-1000 *via* organometallic nickel silylphosphine post-synthetic complex incorporation†

Juan L. Obeso, ‡[a,b] Luz J. Barrios-Vargas,‡[c] Valeria B. López-Cervantes, ‡[a] Yoarhy A. Amador-Sánchez,[a] Nancy Martin-Guaregua,[d] Ricardo A. Peralta, [d] Ramon Munoz,[e] Ana Martínez, [f] Carolina Leyva, [b] Diego Solis-Ibarra, [a] Elí Sánchez-González, *[a] Ilich A. Ibarra *[a] and Virginia Montiel-Palma *[c]

The adsorption and detection of SO_2 using Zr-based MOF, NU-1000 grafted with an organometallic nickel silylphosphine complex ([NiSi]@NU-1000) *via* post-synthetic modification are reported. [NiSi]@NU-1000 exhibits high stability under dry and wet SO_2, with a high cyclability performance. Moreover, fluorescence experiments postulate [NiSi]@NU-1000 as a promising SO_2 detector due to its high SO_2 selectivity over CO_2 and air, showing an evident quenching effect, especially at low SO_2 concentrations (0.1 bar of SO_2). Time-resolved photoluminescence experiments suggest that host–guest SO_2 interactions are associated with the turn-off effect.

Sulphur dioxide (SO_2) is an irritant, colourless gas at ambient temperature and pressure and is classified as a primary pollutant because it is released directly into the atmosphere.[1] It is naturally emitted by volcanic activity and fires (forest and agricultural).[2] However, the major source of this gas is anthropogenic from power plants, oil refineries, and smelters. Its emissions are of concern because of their adverse effects on human health and the environment.[3] Currently, most of the flue gas desulphurisation (FGD) technologies are based on the absorption of SO_2 in wet alkaline scrubbers. Despite their effectiveness, these systems have highly energetic regeneration conditions, and their by-products generate corrosion.[4] Thereby, another alternative for capturing toxic gases is adsorption, which uses less energy and minimises waste.[5]

Most research efforts concerning SO_2 have concentrated on its capture. However, due to the danger it poses to human health, many industries need accurate detection methods for SO_2 to prevent it from reaching toxic levels.[6] Currently, the detection of SO_2 in ambient air has been carried out by colourimetric,[7] conductimetric,[8] and fluorescent methods.[9] Fluorescence-based chemical detectors stand out due to their simplicity, sensitivity, nontoxicity, and ease of operation.[10] In this context, MOFs are a class of hybrid materials composed of metal clusters intertwined by organic linkers,[11] which have emerged as viable platforms to detect pollutants in water and air.[6] Mainly, applying MOF materials as fluorescent detectors for small molecules or conjugated polymers is innovative. Moreover, MOFs display chemical tunability, resulting in efficient and specific recognition, and their structures are rich in π and n electrons, which are conducive to forming excellent and variable fluorescence signals.[12] MOF active site dispersion is suitable for an outstanding guest–host interaction, which can generate a turn-on or turn-off in the luminescence of the material due to the rearrangement of electrons within the MOFs.[13,14] Therefore, it is crucial to have a relatively strong interaction between the gas and the material to obtain a fluorescence response. Interestingly, incorporating additional adsorption sites in a MOF can generate a higher energy transfer, causing a significant change in its fluorescence properties.[15]

As a ligand to transition metals, the SO_2 molecule exhibits three main coordination modes: planar η^1-S and η^2-S, O when it acts as a Lewis base, and a pyramidal η^1-S mode when it acts as a Lewis acid, and since the energy barriers for interconversion

[a]*Laboratorio de Fisicoquímica y Reactividad de Superficies (LaFReS), Instituto de Investigaciones en Materiales, Universidad Nacional Autónoma de México, Circuito Exterior s/n, CU, Coyoacán, 04510 Ciudad de México, Mexico. E-mail: argel@unam.mx, elisg@materiales.unam.mx*
[b]*Instituto Politécnico Nacional, CICATA U. Legaria, Laboratorio Nacional de Ciencia, Tecnología y Gestión Integrada del Agua , (LNAgua), Legaria 694 Irrigación, Miguel Hidalgo, CDMX, Mexico*
[c]*Department of Chemistry, Mississippi State University, Mississippi State, Mississippi 39762, USA. E-mail: vmontiel@chemistry.msstate.edu*
[d]*Departamento de Química, División de Ciencias Básicas e Ingeniería, Universidad Autónoma Metropolitana Unidad Iztapalapa (UAM-I), 09340, Mexico*
[e]*Mississippi School for Maths and Science, 1100 College St, Columbus, Mississippi 39701, USA*
[f]*Departamento de Materiales de Baja Dimensionalidad. Instituto de Investigaciones en Materiales, Universidad Nacional Autónoma de México, Circuito Exterior s/n, CU, Coyoacán, 04510 Ciudad de México, Mexico*

† Electronic supplementary information (ESI) available: Instrumental techniques and characterization. See DOI: **https://doi.org/10.1039/d3dt03985d**

‡ These authors contributed equally to this manuscript.

are relatively small, a planar η^1-S/η^2-S,O isomerisation can readily occur.[16–18] Accordingly, we have previously reported enhancement of the reversible SO_2 uptake in MOF material NU-1000 by incorporation of organometallic moieties of precious metals Ru[19] and Ir.[20] Grafting of the organometallic fragment enhances the uptake of SO_2 by the MOF material due to the accessibility of additional coordination sites. In parallel, preservation of the porosity of the MOF material and recyclability for up to 10 adsorption/desorption cycles make those materials attractive.

Herein, we have now employed the grafted NU-1000 with an earth-abundant base metal complex derived from a silicon-substituted triphosphine ligand, [HNi(κ^4(Si,P,P,P)-Si(*o*-$C_6H_4CH_2PPh_2)_3$)], herein entitled [NiSi]@NU-1000 (Fig. 1), for the adsorption and detection of SO_2. The material exhibits outstanding fluorescence properties with high selectivity and remarkable cyclability.

[NiSi]@NU-1000 (Scheme S1†) was synthesised reported[21] and obtained as a yellow powder; its crystalline structure was corroborated by PXRD (Fig. S6†). The presence of the [NiSi] complex was ascertained by a variety of techniques, including FT-IR and ^{1}H NMR of the digested sample (Fig. S12 and S13†). XANES and SEM analyses are consistent with Ni in oxidation state of +2 and with the homogeneous distribution of the Ni complex through the material (Fig. S7 and S8†).

[NiSi]@NU-1000 displays moderate thermal stability up to 300 °C (Fig. S10†). The Ni and Zr contents were verified by ICP-MS as 0.6 wt% and 5.4 wt% respectively, corresponding to a Ni : Zr molar ratio of *ca.* 1 : 6, very close to the ideal one Ni atom per Zr_6 cluster unit of the NU-1000 material.[21] The BET surface area decreased from 1970 $m^2\ g^{-1}$ in the as-synthesized NU-1000 to 1354 $m^2\ g^{-1}$ in [NiSi]@NU-1000 in accordance with grafting of the organometallic complex onto the MOF (Fig. S6†).[21] We propose that upon grafting, the structure of the Ni silylphosphine complex is maintained, and the Ni centre binds to the zirconium node through a terminal hydroxyl group.[21] Solid-state UV-Vis of [NiSi]@NU-1000 (Fig. S11†) exhibits a maximum adsorption peak at 420 nm.

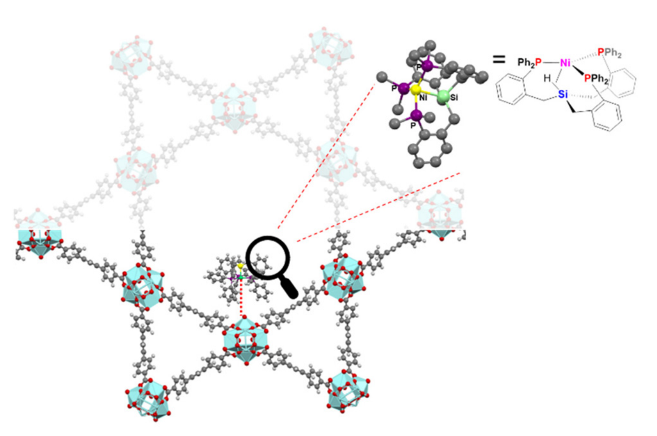

Fig. 1 Structure representation of NU-1000 post-synthetically grafted with a nickel phosphinosilyl complex. Atom label: light blue: Zr, yellow: Ni, dark grey: carbon, light grey; hydrogen, purple: P and green: Si.

Prior to adsorption experiments, [NiSi]@NU-1000 was activated at 120 °C under vacuum for 24 h to release the pores. Fig. 2 shows the SO_2 adsorption–desorption isotherm. First, rapid capture from 0 to 0.01 bar of 0.52 mmol g^{-1} is observed, followed by a linear capture with a total amount of 2.48 mmol g^{-1} at 0.5 bar. This performance has been observed for mesoporous materials because the saturation of the material is not achieved at the experimental conditions.[19,20] The isotherm shows a desorption step with a slight hysteresis, indicating that SO_2 was completely released from the sample, and a relatively low SO_2-MOF interaction can be inferred.[22] Moreover, to explore its potential application in SO_2 detection, the adsorption in the low-pressure range was analysed. It is important to highlight that adsorption in the low-pressure range can be associated with low SO_2 concentrations (ppm levels).[23] At low pressures (<0.01 bar), the [NiSi]@NU-1000 material shows a higher adsorption uptake in comparison with the unmodified NU-1000 material (Fig. S14†). This could be due to the higher affinity of the organometallic moiety for SO_2 coordination.[19] At higher pressures, the presence of the organometallic restricts access to the pores, resulting in a decrease in the adsorption capacity compared to the unmodified material (Fig. S14†). The [NiSi]@NU-1000 outperforms the SO_2 uptake at 0.002 bar (0.40 mmol g^{-1}) of NU-1000, [Ir]@NU-1000,[20] [RuGa]@NU-1000,[19] DUT-67(Zr),[24] Zr-DMTDC, UiO-66, and MFM-133,[25] all of which contain Zr-based SBUs and have surface areas above 1000 $m^2\ g^{-1}$ (Table S2†). Nonetheless, [NiSi]@NU-1000 falls short of the best-performing MOF, Mg-gallate, with an SO_2 uptake of 4.65 mmol g^{-1} at 0.002 bar.[26]

Cycling SO_2 experiments were conducted at 0.05–0.1 bar and 298 K (Fig. 2, inset). Each regeneration process was per-

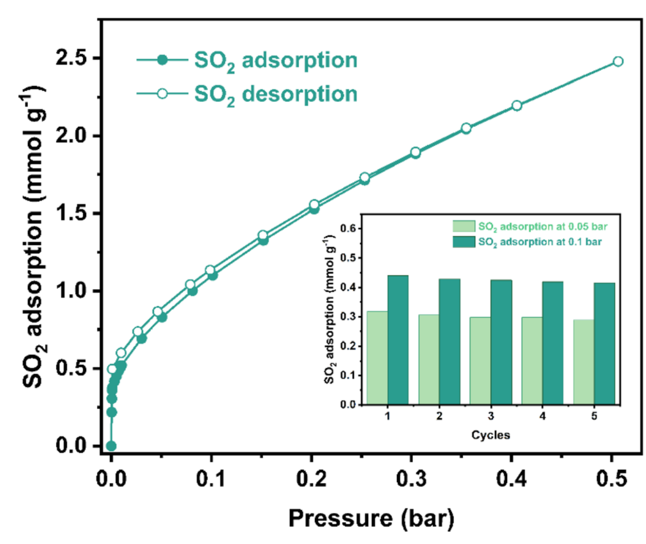

Fig. 2 Experimental SO_2 adsorption–desorption isotherm collected for a fully activated [NiSi]@NU-1000 sample (filled green diamonds = adsorption; open green diamonds = desorption) at 298 K and up to 0.5 bar. Inset: adsorption–desorption cycles for SO_2 in [NiSi]@NU-1000 at 0.05–0.1 bar and 298 K. The reactivation step was carried out only by applying vacuum (1.7×10^{-3} torr) for 45 minutes at room temperature (298 K).

formed under vacuum (1.7×10^{-3} Torr) for 45 minutes and 298 K. It was observed that even after five adsorption–desorption experiments, the SO_2 uptake was maintained at 0.05 and 0.1 bar. This confirms complete SO_2 release during the desorption cycles. PXRD measurements corroborated the retention of the crystallinity (Fig. S15†) and the material's stability after the SO_2 adsorption and cyclability test. Energy-dispersive X-ray spectroscopy (EDX) analyses showed no evidence of changes in the amount of Ni before and after the SO_2 experiments, highlighting the stability of the isolated metal complex within the MOF framework (Table S3†). Moreover, the presence of sulphur within the MOF was corroborated, revealing that the calculated amount is two times more than expected only from the incorporated metal complex and supporting that the uptake of SO_2 takes place in different parts of the MOF framework, and not exclusively in the Ni centre. Also, the stability of [NiSi]@NU-1000 under wet SO_2 was tested. An activated sample was exposed for 3 h to humid SO_2 (exposure at 60% relative humidity, RH), generated in a home-designed setup (Fig. S20†). It was observed by PXRD that the crystalline structure was maintained (Fig. S15†).

The host–guest interaction between SO_2 and [NiSi]@NU-1000 was elucidated by calculating the isosteric enthalpy of adsorption (ΔH_{ads}) for SO_2 at low coverage for a fully activated sample using the virial method (Fig. S19†).[27] The calculated ΔH_{ads} at low coverage was −42.7 kJ mol^{-1}; such value corresponds to a physisorption, in line with the reversible adsorption/desorption cycles and easy desorption step, only with vacuum. The decrease in the enthalpy of adsorption of [NiSi]@NU-1000 compared to the pristine NU-1000 (−50.8 kJ mol^{-1}),[20] could be attributed to both the high metal content (1 : 1, Ni per Zr_6 cluster) and the steric bulk of the silicon-substituted triphosphine ligand in the [NiSi] complex. These values of enthalpies of adsorption are in agreement with the formation of hydrogen bonds between SO_2 and the bare $[Zr_6(\mu_3\text{-}OH)_8(OH)_8]$ cluster as well as the establishment of electrostatic interactions between the SO_2 and the grafted [NiSi] complex (Fig. S25†). The pristine NU-1000 material only exhibits hydrogen bond interactions with the SO_2. In contrast, the [NiSi]@NU-1000 material additionally has lower energy SO_2 electrostatic interactions with the [NiSi] complex, accounting for the decrease in the overall enthalpy of adsorption. This weak interaction was confirmed by the FTIR spectrum of an SO_2-loaded sample, which showed some weak bands at 1336 and 1144 cm^{-1} (Fig. S18†); these correspond to adsorbed SO_2, which is slightly redshifted compared to free SO_2 (1362 and 1151 cm^{-1}).[41] In comparison, the previously studied [Ir]@NU-1000 material, an organometallic iridium bis(silyl)phosphine complex grafted onto NU-1000 in a molar ratio 1 : 11 (Ir : Zr_6), exhibited a higher enthalpy of adsorption towards SO_2 (−89.8 kJ mol^{-1}), where chemisorption occurred upon SO_2 bonding with the metal center.[20]

Several properties of MOF materials have been widely employed for the detection of SO_2 gas. SO_2 detection was conducted in Ni_3BTC_2 based on the change in its electrochemical behavior.[28] Also, the detection of SO_2 can be achieved using the change in the magnetic properties related to the spin-crossover transition.[29] However, SO_2 detection using the change in the luminescence properties is an attractive technique for the simplicity of the experiment. Indeed, modifications in the fluorescence performance of several MOF materials including MOF-303, DNA-Tb-MOF and M_2(dobpdc) (M = Ni^{2+} and Mg^{2+}) were investigated using this approach.[9,30–32]

It has been reported that NU-1000 displays photoluminescence properties based on the highly conjugated TBAPy linker, which remains unchanged after coordination with Zr^{4+}.[33] NU-100 has been evaluated to detect pesticides, explosive compounds, and metabolites in aqueous matrices by measuring the "turn-off" effect of these analytes.[34–37] Also, the Ni complex incorporation in NU-1000 displays similar photoluminescence properties. Then, the pore confinement effect improves the detection effectiveness in this material at low pressures. Based on this and the SO_2 adsorption properties of NU-1000 and [NiSi]@NU-1000, the materials were evaluated as fluorescent SO_2 detectors for low pressure.

The fluorescence emission at different excitation wavelengths indicates that the appropriate excitation wavelength for [NiSi]@NU-1000 is 350 nm (Fig. S21†). The solid-state emission spectra of [NiSi]@NU-1000 are shown in Fig. 3a. The activated [NiSi]@NU-1000 sample displays a peak at 497 nm. Then, an activated [NiSi]@NU-1000 sample was exposed to 0.1 bar of SO_2. Interestingly, a "turn-off" effect is observed with a 3.65-decreased fold in emission intensity compared to the activated sample. In order to corroborate the stability in the emission of [NiSi]@NU-1000, a cycling test was performed (Fig. S22†).

Five cycle experiments were conducted, observing that the emission in both cases was maintained. The SO_2-exposed [NiSi]@NU-1000 shows a constant "turn-off" effect with an average 3.65 ± 0.03-fold decrease in emission intensity. Furthermore, the fluorescence of [NiSi]@NU-1000 upon exposure to air (which contains ∼78%) and CO_2 was investigated to determine the selectivity (Fig. 3a). By comparison, a slight change in the fluorescence intensity is observed. However, higher selectivity is clearly observed for SO_2 molecules. This can be attributed to the non-polar character of the CO_2 and N_2 molecules, which makes their interaction with the adsorption sites of the material unfavourable, whereas SO_2, being a polar molecule, can establish specific interactions with the material, resulting in a quenching effect on the fluorescence.

This high selectivity of [NiSi]@NU-1000 for SO_2 can be related to improved host–guest interactions due to the grafting of the organometallic species. As a comparison, the fluorescence performances for NU-1000 and [NiSi]@NU-1000 before and after SO_2 were tested (Fig. S23†). A slight shift in the emission maxima (5 nm) for the grafted material was observed compared to the pristine material, indicating the photoluminescent properties are mainly due to the pyrene core linker. A turn-off phenomenon was observed for both materials. It is evident, however, that grafted [NiSi]@NU-1000

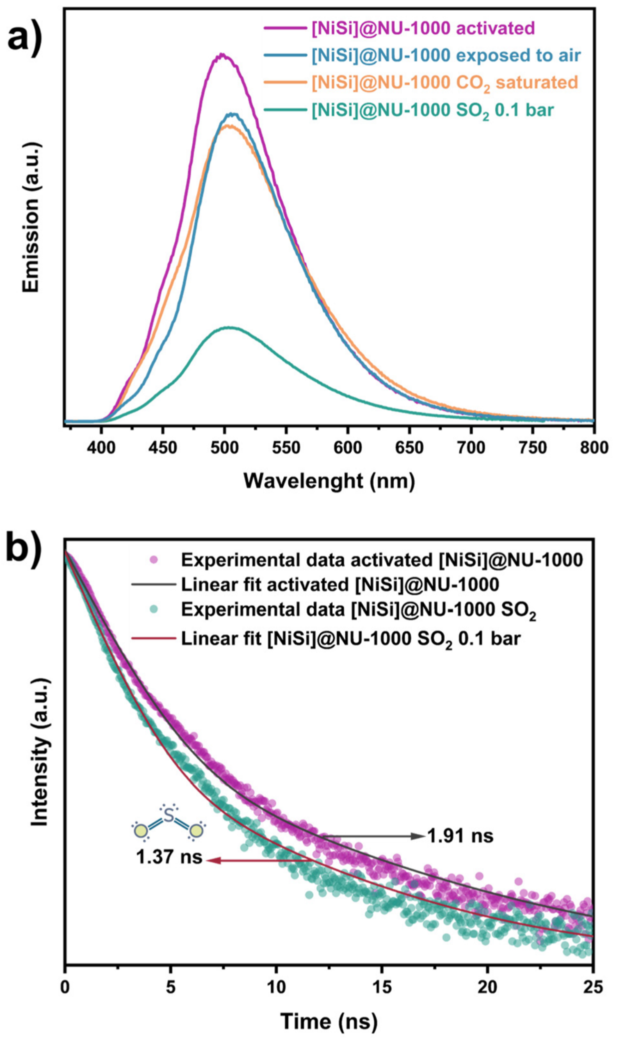

Fig. 3 (a) Solid-state emission spectra of activated [NiSi]@NU-1000 (purple line), and after exposure to 0.1 bar of SO_2 (green line), CO_2 (orange line), and air (blue line). The excitation wavelength was set at 350 nm, (b) time-resolved photoluminescence decay spectra of activated [NiSi]@NU-1000, and after exposure to 0.1 bar of SO_2 measured at 335.6 nm excitation and at 500 nm emission.

considerably improves the fluorescence response by turning off the response by almost 75%.

It has been reported that in NU-1000 materials, hydrogen bonding and π–π interactions could generate a quenching effect.[36] One possible explanation is that the presence of the [NiSi] complex within NU-1000 reversibly bonding SO_2 brings about a higher amount of SO_2 molecules into the MOF pore walls, triggering SO_2 packing and increasing π-SO_2 interactions in the vicinity of the pyrene linkers thus turning off the fluorescence response. The proposed hydrogen-bond interactions of SO_2 with [NiSi]@NU-1000 are illustrated in Fig. S24.†

Furthermore, a time-resolved photoluminescence (TRPL) experiment was performed using a 340 nm picosecond-pulsed LED as the excitation source (Fig. 3b) to investigate the possible SO_2 detection. TRPL experiments were conducted on an activated [NiSi]@NU-1000 and an SO_2-exposed sample. It was observed that the average decay lifetimes (Table S4†) slightly decreased from 1.91 to 1.37 ns from activated [NiSi]@NU-1000 and an SO_2-exposed, respectively (a decrease of 28% in the fluorescence lifetime). This decrease can be explained by analysing the individual lifetime components (τ_n) and their contributions (a_n). Table S3† shows that, in all cases, τ_1 is the shortest lifetime component, which can be associated with fast non-radiative relaxation processes, which occur in orders of less than nanoseconds,[38] or very effective interactions. After SO_2 adsorption, the relative contribution (a_1) of this short component increases slightly, from 0.24 to 0.32, indicating that fast relaxation processes become slightly more relevant, coinciding with the observed decrease in fluorescence intensity. On the other hand, τ_3, the longest lifetime component, is associated with slower phenomena, such as radiative mechanisms that occur on the order of nanoseconds.[39] This component decreases both in its value, from 5.4 to 4.3 ns, as its relative contribution, from 0.21 to 0.17, after SO_2 adsorption. This suggests that the interaction with SO_2 induces non-radiative relaxation processes in species with longer lifetimes. This pathway could be associated with an electron transfer phenomenon related to the direct interaction between SO_2 and the surface of the grafted [NiSi] complex, which deactivates the excited states in a non-radiative manner.[14,40]

To further support this analysis, we performed TRPL experiments for the NU-1000 material, comparing it with its modified analogue, [NiSi]@NU-1000. The data (Table S4†) reveal that, in NU-1000, the fluorescence lifetime decreases from 2.23 to 1.75 ns after SO_2 adsorption, corresponding to a reduction of 21.5%. In comparison, [NiSi]@NU-1000 shows a more pronounced decrease of 28%. Similarly, the relative contributions of the lifetime components show more pronounced changes in [NiSi]@NU-1000. This indicates that the [NiSi] complex intensifies the non-radiative dissipation pathways, enhancing the sensitivity of the material to SO_2 adsorption. Regarding the possible influence of absorption on fluorescence quenching, we collected solid-state UV-Vis diffuse reflectance spectra for the activated, SO_2-exposed, and desorbed [NiSi]@NU-1000 samples (Fig. S11†). The spectra show that the absorption region of the material, as well as the relative intensity at the excitation wavelength (~340 nm), do not change significantly after SO_2 adsorption. This suggests that the decrease in fluorescence intensity is not related to a reduction in absorption at the excitation wavelength but to non-radiative processes associated with direct electronic interactions between SO_2 and the active sites of the material.

This study investigated the SO_2 adsorption and detection properties of a nickel silylphosphine organometallic complex post-synthetic grafted to a Zr-based MOF ([NiSi]@NU-1000). The material shows high stability to wet and dry SO_2. Furthermore, high cyclability at the low-pressure range was achieved with a facile SO_2 regeneration at room temperature. Fluorescence studies display a remarkable change in the intensity from the emission spectra after the SO_2 interactions with the material and high selectivity over CO_2 and air, and an evident SO_2 quenching effect is observed even at low concentrations (0.1 bar of SO_2). Finally, time-resolved photoluminescence experiments suggest that the turn-off effect is associated with relatively strong host–guest SO_2 interactions.

Data availability

All data is available in the main text and in the ESI.†

Conflicts of interest

There are no conflicts to declare.

Acknowledgements

J. L. O. and V. B. L.-C. thank CONAHCYT for the Ph.D. fellowships (1003953 and 1005649). R. A. P. thanks the Autonomous University of Mexico-Iztapalapa, Mexico, for the financial support. We thank U. Winnberg (Euro Health) for scientific discussions and G. Ibarra-Winnberg for scientific encouragement. I. A. I. thanks PAPIIT UNAM (IN201123), México, for financial support. A. M. thanks to LANCAD-UNAM-DGTIC-141 for computer facilities. V. M. P. thanks the Division of Chemistry of the National Science Foundation, NSF, for financial support through project 2102689 and Dr Zamora-Moreno for technical assistance.

References

1 J. A. Bernstein, N. Alexis, C. Barnes, I. L. Bernstein, A. Nel, D. Peden, D. Diaz-Sanchez, S. M. Tarlo, P. B. Williams and J. A. Bernstein, *J. Allergy Clin. Immunol.*, 2004, **114**, 1116–1123.
2 J. Roberge, H. Delgado-Granados and P. J. Wallace, *Geology*, 2009, **37**, 107–110.
3 J. S. Pandey, R. Kumar and S. Devotta, *Atmos. Environ.*, 2005, **39**, 6868–6874.
4 R. K. Srivastava, W. Jozewicz and C. Singer, *Environ. Prog.*, 2001, **20**, 219–228.
5 J. L. Obeso, D. R. Amaro, C. V. Flores, A. Gutiérrez-Alejandre, R. A. Peralta, C. Leyva and I. A. Ibarra, *Coord. Chem. Rev.*, 2023, **485**, 215135.
6 H. Sohrabi, S. Ghasemzadeh, Z. Ghoreishi, M. R. Majidi, Y. Yoon, N. Dizge and A. Khataee, *Mater. Chem. Phys.*, 2023, **299**, 127512.
7 A. V. Leontiev and D. M. Rudkevich, *J. Am. Chem. Soc.*, 2005, **127**, 14126–14127.
8 G. Zhang, Z. Wang and X. Zhang, *Mol. Phys.*, 2022, **120**, e2018517.
9 V. B. López-Cervantes, D. W. Kim, J. L. Obeso, E. Martínez-Ahumada, Y. A. Amador-Sánchez, E. Sánchez-González, C. Leyva, C. S. Hong, I. A. Ibarra and D. Solis-Ibarra, *Nanoscale*, 2023, **15**, 12471–12475.
10 F. Wu, J. Ye, Y. Cao, Z. Wang, T. Miao and Q. Shi, *Luminescence*, 2020, **35**, 440–446.
11 S. L. James, *Chem. Soc. Rev.*, 2003, **32**, 276–288.
12 T. Wu, X. Gao, F. Ge and H. Zheng, *CrystEngComm*, 2022, **24**, 7881–7901.
13 X. Dou, K. Sun, H. Chen, Y. Jiang, L. Wu, J. Mei, Z. Ding and J. Xie, *Antibiotics*, 2021, **10**, 358.
14 J.-X. Wang, J. Yin, O. Shekhah, O. M. Bakr, M. Eddaoudi and O. F. Mohammed, *ACS Appl. Mater. Interfaces*, 2022, **14**, 9970–9986.
15 D. Mahato, S. Fajal, P. Samanta, W. Mandal and S. K. Ghosh, *ChemPlusChem*, 2022, **87**, e202100426.
16 J. Li and A. Y. Rogachev, *Phys. Chem. Chem. Phys.*, 2015, **17**, 1987–2000.
17 W. A. Schenk, *Dalton Trans.*, 2011, **40**, 1209–1219.
18 A. V. Marchenko, A. N. Vedernikov, J. C. Huffman and K. G. Caulton, *New J. Chem.*, 2003, **27**, 680–683.
19 J. García Ponce, M. L. Díaz-Ramírez, S. Gorla, C. Navarathna, G. Sanchez-Lecuona, B. Donnadieu, I. A. Ibarra and V. Montiel-Palma, *CrystEngComm*, 2021, **23**, 7479–7484.
20 S. Gorla, M. L. Díaz-Ramírez, N. S. Abeynayake, D. M. Kaphan, D. R. Williams, V. Martis, H. A. Lara-García, B. Donnadieu, N. Lopez, I. A. Ibarra and V. Montiel-Palma, *ACS Appl. Mater. Interfaces*, 2020, **12**, 41758–41764.
21 L. J. Barrios-Vargas, N. S. Abeynayake, C. Secrist, N. Le, C. E. Webster, B. Donnadieu, D. M. Kaphan, A. D. Roy, I. A. Ibarra and V. Montiel-Palma, *Dalton Trans.*, 2023, **52**, 8883–8892.
22 E. Martínez-Ahumada, A. López-Olvera, V. Jancik, J. E. Sánchez-Bautista, E. González-Zamora, V. Martis, D. R. Williams and I. A. Ibarra, *Organometallics*, 2020, **39**, 883–915.
23 S. Xing, J. Liang, P. Brandt, F. Schäfer, A. Nuhnen, T. Heinen, I. Boldog, J. Möllmer, M. Lange, O. Weingart and C. Janiak, *Angew. Chem., Int. Ed.*, 2021, **60**, 17998–18005.
24 P. Brandt, S. H. Xing, L. Liang, G. Kurt, A. Nuhnen, O. Weingart and C. Janiak, *ACS Appl. Mater. Interfaces*, 2021, **13**, 29137–29149.
25 J. Li, G. L. Smith, Y. Chen, Y. Ma, M. Kippax-Jones, M. Fan, W. Lu, M. D. Frogley, G. Cinque, S. J. Day, S. P. Thompson, Y. Cheng, L. L. Daemen, A. J. Ramirez-Cuesta, M. Schröder and S. Yang, *Angew. Chem., Int. Ed.*, 2022, **61**, e2022072.
26 F. Chen, D. Lai, L. Guo, J. Wang, P. Zhang, K. Wu, Z. Zhang, Q. Yang, Y. Yang, B. Chen, Q. Ren and Z. Bao, *J. Am. Chem. Soc.*, 2021, **143**, 9040–9047.
27 A. Nuhnen and C. Janiak, *Dalton Trans.*, 2020, **49**, 10295–10307.
28 N. Ingle, S. Mane, P. Sayyad, G. Bodkhe, T. Al-Gahouari, M. Mahadik, S. Shirsat and M. D. Shirsat, *Front. Mater.*, 2020, **7**, 93.
29 C. H. Pham and F. Paesani, *Inorg. Chem.*, 2018, **57**, 9839–9843.

30 Y. Xie, H. Ma, F. L. He, J. Chen, Y. Ji, S. Han and D. Zhu, *Analyst*, 2020, **145**, 4772–4776.

31 E. Martínez-Ahumada, D. W. Kim, M. Wahiduzzaman, P. Carmona-Monroy, A. López-Olvera, D. R. Williams, V. Martis, H. A. Lara-García, S. López-Morales, D. Solis-Ibarra, G. Maurin, I. A. Ibarra and C. S. Hong, *J. Mater. Chem. A*, 2022, **10**, 18636–18643.

32 J. L. Obeso, E. Martínez-Ahumada, A. López-Olvera, J. Ortiz-Landeros, H. A. Lara-García, J. Balmaseda, S. López-Morales, E. Sánchez-González, D. Solis-Ibarra, C. Leyva and I. A. Ibarra, *ACS Appl. Energy Mater.*, 2023, **6**, 9084–9091.

33 P. Deria, J. Yu, T. Smith and R. P. Balaraman, *J. Am. Chem. Soc.*, 2017, **139**, 5973–5983.

34 Y. Zhou, Q. Yang, J. Cuan, Y. Wang, N. Gan, Y. Cao and T. Li, *Analyst*, 2018, **143**, 3628–3634.

35 W. Hao, G. Huang, G. Jiang, S. A. Dauda and F. Pi, *Food Biosci.*, 2023, **55**, 102967.

36 H. Li, Q. Chen, Z. Zhang, Z. Wang, Z. Gong and M. Fan, *Dyes Pigm.*, 2023, **210**, 111035.

37 F. Gabriel, A. Roussey, S. Sousa Nobre and A. Carella, *J. Mater. Chem. C*, 2024, **12**, 11378–11385.

38 B. Valeur and M. N. Berberan-Santos, *Molecular Fluorescence*, Wiley, 2012.

39 U. Noomnarm and R. M. Clegg, *Photosynth. Res.*, 2009, **101**, 181–194.

40 P. Chandrasekhar, A. Mukhopadhyay, G. Savitha and J. N. Moorthy, *Chem. Sci.*, 2016, **7**, 3085–3091.

41 A. L. Goodman, P. Li, C. R. Usher and V. H. Grassian, *J. Phys. Chem. A*, 2001, **105**, 6109–6120.